

# Upconversion luminescence of Er, Yb – doped nanolanganite powders synthesized by a citrate sol-gel method

A. M. VOICULESCU\*, S. GEORGESCU, O. TOMA, S. NASTASE, R. BIRJEGA, L. PETRESCU<sup>a</sup>, I. ENCULESCU<sup>b</sup>, E. MATEI<sup>b</sup>

*National Institute for Laser, Plasma and Radiation Physics, Măgurele, Ilfov, Romania*

<sup>a</sup>*Faculty of Biology, University of Bucharest, Bucharest, Romania*

<sup>b</sup>*National Institute for Materials Physics, Măgurele, Ilfov, Romania*

Langanite nanopowders doped with erbium and ytterbium were prepared by a citrate sol–gel method and annealed in air at various temperatures between 700°C and 1000°C. For annealing temperatures 900°C and 1000°C, part of the langanite transforms in perovskite (LaGaO<sub>3</sub>), as evidenced in XRD spectra. The reddish color of the powders due to color centers associated to oxygen defects intensifies with increasing annealing temperature. Green and red luminescence was obtained for IR (933 nm) pumping and only green for UV pump. The mechanisms involved in luminescence and energy transfer processes are presented and discussed.

(Received October 31, 2011; accepted November 23, 2011)

*Keywords:* Langanite, Er<sup>3+</sup>, Yb<sup>3+</sup>, Upconversion, Luminescence

## 1. Introduction

The crystals from the langasite family were initially intended as host for laser active media [1], but in present their main application is based on their very good piezoelectric characteristics [2, 3].

The crystals from the langasite family, langasite (La<sub>3</sub>Ga<sub>5</sub>SiO<sub>14</sub> – LGS), langanite (La<sub>3</sub>Ga<sub>5.5</sub>Nb<sub>0.5</sub>O<sub>14</sub> – LGN) and langatate (La<sub>3</sub>Ga<sub>5.5</sub>Ta<sub>0.5</sub>O<sub>14</sub> – LGT) – generic LGX – are partially disordered, i.e. one of the crystallographic positions is occupied by two different ions. The structure of these crystals is given by the formula  $A_3BC_3D_2O_{14}$  where *A* represents the dodecahedral positions (distorted Thompson cubes), *B* – octahedral positions and *C*, *D* – tetrahedral positions. La<sup>3+</sup> occupies the position *A*. The local symmetry at this site is C<sub>2</sub>. In LGS, the *D* positions are randomly occupied by Ga<sup>3+</sup> and Si<sup>4+</sup> while in LGN (LGT) Nb<sup>5+</sup> (Ta<sup>5+</sup>) and Ga<sup>3+</sup> occupy the *B* positions.

Recently, we discussed the emission properties of Eu<sup>3+</sup> in langanite nanocrystals [4]. When excited in the near UV (395 nm), these nanocrystals show bright red luminescence which suggests the possibility to use these materials as red phosphors.

To our best knowledge, the upconversion luminescence in nanocrystals from the langasite family doped with Yb<sup>3+</sup> and Er<sup>3+</sup> has not been reported. In this paper we present preliminary data concerning synthesis and characterization of Er, Yb-doped LGN nanocrystals obtained by a citrate sol-gel synthesis.

## 2. Experimental

Details concerning the synthesis of the langanite nanopowder by the citrate sol-gel method can be found in [5]. In this paper, instead of europium nitrate, erbium nitrate and ytterbium nitrate are used. The final formula is (La<sub>0.95</sub>Er<sub>0.01</sub>Yb<sub>0.04</sub>)<sub>3</sub>Ga<sub>5.5</sub>Nb<sub>0.5</sub>O<sub>14</sub>. The resulting powders were annealed five hours in air at 700°C, 800°C, 900°C and 1000°C.

XRD measurements were performed on a PANalytical X'Pert PRO MPD diffractometer (CuK $\alpha$ ). The fluorescence of the Er:Yb:LGN was excited in UV using a ScienceTech Xe-Hg 350-W lamp with suitable filters and in IR at 933 nm with laser diode JOLD-200-CABN-4A. The luminescence spectra were measured using a Horiba Jobin-Yvon 1000M monochromator, an S-20 photomultiplier and an SR830 lockin amplifier. The experimental setup for diffuse reflectance measurements was described elsewhere [6]. All measurements were performed at room temperature.

## 3. Results and discussion

### 3.1. XRD

In Fig. 1 are given the XRD patterns of the Er, Yb-doped LGN powders annealed at temperatures between 700 °C, 800 °C, 900 °C, and 1000 °C. For the samples annealed at 700°C and 800 °C, besides the diffraction lines belonging to the LGN phase (card PDF-00-047-0533), there are other extra lines (denoted by small circles) which disappear at higher annealing temperatures.

For the samples annealed at 900°C and 1000°C, besides the LGN lines, diffraction lines of the perovskite phase ( $\text{LaGaO}_3$  - PDF 01-072-8227) are present, their intensity increasing with annealing temperature. The presence of  $\text{LaGaO}_3$  diffraction lines was also observed in europium-doped nanolanganite annealed at 1000°C [4]. As the thermal treatment temperature increases, the LGN and  $\text{LaGaO}_3$  diffraction lines became narrower, indicating an improved crystallinity of the nanopowders.

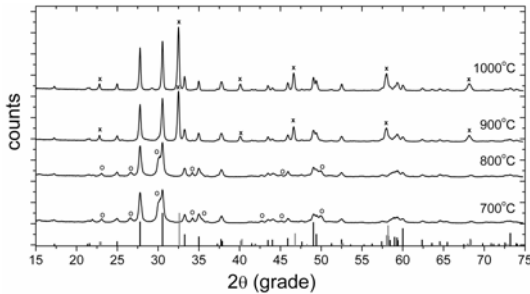


Fig. 1. XRD patterns of LGN:Yb:Er nanopowders. The diffraction lines belonging to LGN phase (card PDF-00-047-0533, black bars at the bottom) and  $\text{LaGaO}_3$  denoted by x's (card PDF 01-072-8227, gray bars at the bottom), are identified. The other extra-lines (small circles) disappear at higher calcination temperatures.

The size (coherent domain size) of the nanoparticles can be estimated with the Scherrer formula. The LGN nanoparticles increase from ~48 nm at 700 °C to ~87 nm at 1000°C while the size of the  $\text{LaGaO}_3$  nanoparticles varies from ~71 nm at 900 °C to ~77 nm at 1000 °C.

### 3.2. Diffuse reflectance spectra

The diffuse reflectance spectra of the synthesized powders annealed at 700°C, 800°C, 900°C, and 1000°C, in the visible domain (400-700 nm), are given in Fig. 2a. The absorption lines of  $\text{Er}^{3+}$  are indicated. The diffuse reflectance curves are tilted toward shorter wavelengths, due to the presence of defects involving oxygen [7-9]. The most tilted diffuse reflectance curve corresponds to the sample annealed at 1000°C. Increasing the calcination temperature, the absorption due to defects oxygen involving become dominant at shorter wavelengths.

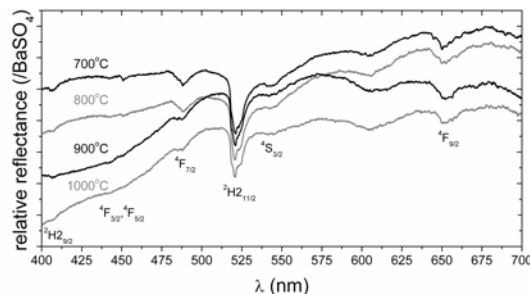


Fig. 2a. VIS diffuse reflectance spectra of LGN:Er:Yb powders annealed at various temperatures.  $\text{BaSO}_4$  is the white etalon.

The infrared diffuse reflectance spectra of the powders annealed at 700 °C, 800 °C, 900 °C, and 1000 °C are shown in Fig. 2b. At ~980 nm the  $\text{Yb}^{3+}$  transition  $^2F_{7/2} \rightarrow ^2F_{5/2}$  is superposed with the  $\text{Er}^{3+}$  transition  $^4I_{15/2} \rightarrow ^4I_{11/2}$ . The narrow features at ~950 nm are due to absorption of atmospheric water vapors.

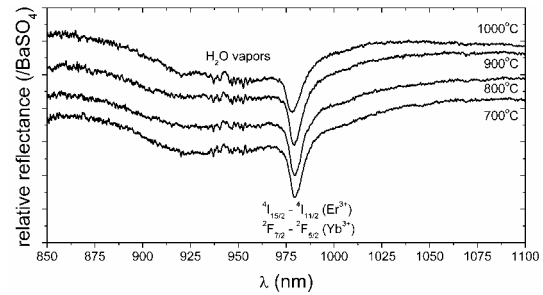


Fig. 2b. IR diffuse reflectance spectra of LGN nanopowders. The spectra are displaced on the vertical scale for more clarity.

Though the analyzed powders contain, besides the LGN phase other phases, as the XRD patterns show, the spectra in Fig. 2b reflect mainly the  $\text{Yb}^{3+}$  absorption in LGN. In fact, the ytterbium concentration is four times larger than the erbium one and the absorption cross section of  $\text{Yb}^{3+} \ ^2F_{7/2} \rightarrow ^2F_{5/2}$  transition is larger than of  $\text{Er}^{3+} \ ^4I_{15/2} \rightarrow ^4I_{11/2}$  one. The shape of spectra in Fig. 2b is close to the absorption spectrum of  $\text{Yb}^{3+}$  in LGT single crystal [10].

### 3.2. Luminescence spectra

In Fig. 3 are given the luminescence spectra excited in UV (at ~400 nm) of the nanopowders annealed at 700°C, 800°C, 900°C, and 1000°C. Due to the very low intensity of the red luminescence ( $^4F_{9/2} \rightarrow ^4I_{15}$ ), only the green part of the spectra (transitions  $^2H_{11/2}, ^4S_{3/2} \rightarrow ^4I_{15/2}$ ) are shown. The shape of the spectra changes with the calcination temperatures due to modification of the phase composition, as the XRD patterns show.

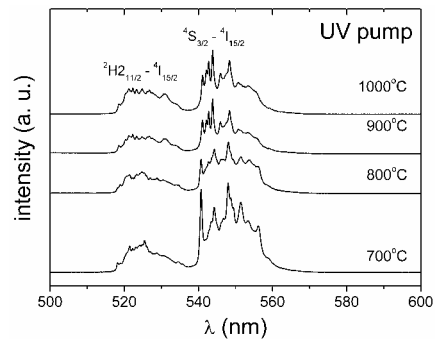


Fig. 3. Luminescence spectra, excited in UV, of LGN:Yb(4%):Er(1%) powders annealed at various temperatures. Due to the very low intensity of the red luminescence ( $^4F_{9/2} \rightarrow ^4I_{15}$ ) only the green part of the spectra are shown. The spectra are not corrected for the spectral responsivity of the experimental apparatus.

In Fig. 4 is represented the integral intensity of the luminescence lines for UV pump function of the thermal treatment temperature. Between 700 °C and 900 °C we observe a net reduction of the luminescence intensity which could be explained by the screening of the absorbing  $\text{Er}^{3+}$  ions at pump wavelengths produced by the color centers. This screening increases with the annealing temperature, as the diffuse reflectance spectra in Fig. 2 show. The increase of the luminescence intensity from 900 °C to 1000 °C could be explained, besides the improvement of the crystallinity and further removing of adsorbed impurities, by the increasing contribution of the perovskite phase which could be more efficient.

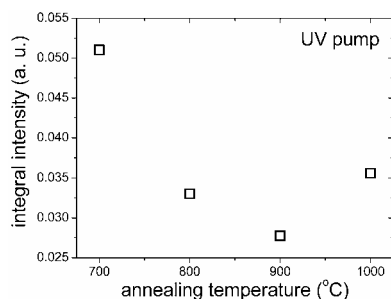


Fig. 4. Integral intensity function of the annealing temperature for UV pumping.

The luminescence spectra for upconversion pump at 933 nm are given in Fig. 5. Increasing the calcination temperature the luminescence intensity increases. The behavior of the integral intensity is shown in Fig. 6. This time, the integral intensity of the luminescence increases monotonically with annealing temperature since at this pump wavelength the screening of the pump radiation by color centers is reduced.

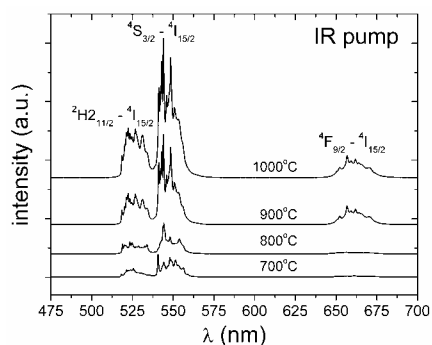


Fig. 5. Luminescence spectra of LGN:Yb(4%):Er(1%) powder excited in IR (933nm). Besides the green luminescence ( ${}^2\text{H}_{211/2}$ ,  ${}^4\text{S}_{3/2} \rightarrow {}^4\text{I}_{15/2}$ ), red luminescence ( ${}^4\text{F}_{9/2} \rightarrow {}^4\text{I}_{15/2}$ ) is observed. The spectra are not corrected for the spectral responsivity of the experimental apparatus.

For IR pump, besides the green luminescence, the red luminescence (transition  ${}^4\text{F}_{9/2} \rightarrow {}^4\text{I}_{15/2}$ ) is also observed. Its

relative intensity in rapport with the green one is higher (approximately two times) for the samples annealed at 900°C and 1000°C.

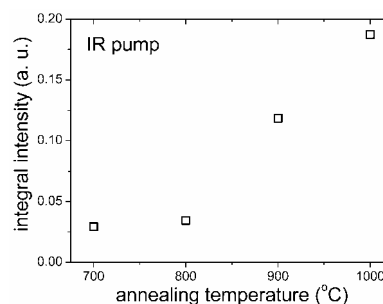


Fig. 6. Integral intensity function of the annealing temperature for IR pumping.

Part of the energy level scheme of  $\text{Yb}^{3+}$  and  $\text{Er}^{3+}$  as well as the main energy transfer processes are sketched in Fig. 7.

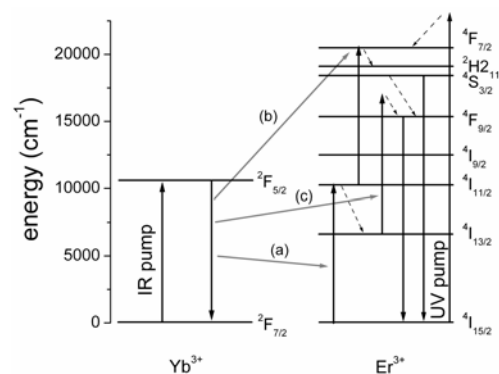


Fig. 7. Energy level diagram of  $\text{Yb}^{3+}$  and  $\text{Er}^{3+}$  in LGT and proposed upconversion mechanisms. Due to the reduced erbium concentration (1 at. %), energy transfer processes between  $\text{Er}^{3+}$  ions can be neglected. The energy transfer processes between  $\text{Yb}^{3+}$  and  $\text{Er}^{3+}$  are indicated by gray arrows. Dashed arrows show multiphonon transitions.

For UV pump, the excitation reaches, via multiphonon transitions, the metastable level  ${}^4\text{S}_{3/2}$  of  $\text{Er}^{3+}$  (thermalized, at room temperature, with  ${}^2\text{H}_{211/2}$ ); the transitions  ${}^4\text{S}_{3/2} \rightarrow {}^4\text{I}_{15/2}$  and  ${}^2\text{H}_{211/2} \rightarrow {}^4\text{I}_{15/2}$  are responsible for the green luminescence. The  ${}^4\text{F}_{9/2}$  level is fed from  ${}^4\text{S}_{3/2}$  via multiphonon transition (see the energy level scheme of  $\text{Er}^{3+}$  and  $\text{Yb}^{3+}$  ions sketched in Fig. 7). Due to the rather narrow energy gap between  ${}^4\text{F}_{9/2}$  and  ${}^4\text{I}_{9/2}$   $\text{Er}^{3+}$  levels, the quantum efficiency of  ${}^4\text{F}_{9/2}$  is usually low, explaining the very weak red luminescence for UV pump. For pumping at 933 nm, the light is absorbed only by  $\text{Yb}^{3+}$ . In Fig. 7 are shown three Yb-Er energy transfer processes: (a)  ${}^2\text{F}_{5/2}$  ( $\text{Yb}^{3+}$ ),  ${}^4\text{I}_{15/2}$  ( $\text{Er}^{3+}$ )  $\rightarrow$   ${}^2\text{F}_{7/2}$  ( $\text{Yb}^{3+}$ ),  ${}^4\text{I}_{11/2}$  ( $\text{Er}^{3+}$ ); as the result of the process (a), the level  ${}^4\text{I}_{11/2}$  ( $\text{Er}^{3+}$ ) is populated. The level  ${}^4\text{I}_{11/2}$  ( $\text{Er}^{3+}$ ) being populated, the process (b)

becomes possible:  ${}^2F_{5/2}(\text{Yb}^{3+}), {}^4I_{11/2}(\text{Er}^{3+}) \rightarrow {}^2F_{7/2}(\text{Yb}^{3+}), {}^4F_{7/2}(\text{Er}^{3+})$ ; from  ${}^4F_{7/2}(\text{Er}^{3+})$ , via multiphonon transitions, the green emitting  $\text{Er}^{3+}$  levels  ${}^4S_{3/2}$  and  ${}^2H_{11/2}$  are populated and it seems that the experimental conditions similar to those obtained for UV pumping are realized. In order to explain the red emission for IR pump, another process should be invoked: (c)  ${}^4F_{5/2}(\text{Yb}^{3+}), {}^4I_{13/2}(\text{Er}^{3+}) \rightarrow {}^2F_{7/2}(\text{Yb}^{3+}), {}^4F_{9/2}(\text{Er}^{3+})$ . This process is not resonant and involves emission of phonons.

#### 4. Conclusions

Nanolanganite powders doped with erbium and ytterbium for upconversion luminescence were synthesized and analyzed for the first time. Green luminescence was obtained for UV pump and bright green an red luminescence was observed for IR (at 933 nm) pump. As the result of thermal treatments in air, the color centers involving oxygen, whose presence increase for higher annealing temperatures, screen the UV pump radiation. For IR pump, where the interference of the pump radiation with the absorption of the color centers is reduced, the visible emission intensity increases with the annealing temperature.

For higher calcination temperatures, part of the LGN transforms in perovskite ( $\text{LaGaO}_3$ ). Studies concerning the stabilization of the langanite phase for higher annealing temperatures and the reduction of the presence of the color centers are now in progress.

#### Acknowledgement

This work was supported by the Romanian National Center for Management of Programs (CNMP), project 62060/2008.

#### References

- [1] A. A. Kaminskii, I. M. Silvestrova, S. E. Sarkisov, G. A. Denisenko, *Phys. Stat. Solid A* **80**, 607 (1983).
- [2] J. Détaint, J. Schwartzel, A. Zarka, B. Capelle, J. P. Denis, E. Phillipot, *Proceedings of the IEEE International Frequency Control Symposium*, 58 (1994).
- [3] R. C. Smythe, R. C. Helmbold, G. E. Hague, K. A. Snow, *IEEE Trans. UFFC* **47**, 355 (2000).
- [4] S. Georgescu, A. M. Voiculescu, O. Toma, S. Nastase, C. Matei, M. Osiac, *J. Alloys Comp.* **507**, 470 (2010).
- [5] F. P. Yu, D. R. Yuan, X. Zhao, S. Y. Guo, X. L. Duan, L. M. Kong, X. Q. Wang, *J. Crystal Growth* **310**, 3256 (2008).
- [6] S. Georgescu, A. M. Voiculescu, O. Toma, C. Tiseanu, L. Gheorghe, A. Achim, C. Matei, *Optoelectron. Adv. Mater.- Rapid Commun.* **3**, 1379 (2009).
- [7] T. Taishi, T. Hayashi, N. Bamba, Y. Ohno, I. Yonenaga, K. Hoshikawa, *Physica B* **401-402**, 437 (2007).
- [8] T. Taishi, T. Hayashi, T. Fukami, K. Hoshikawa, I. Yonenaga, *J. Crystal Growth* **304**, 4 (2007).
- [9] G. M. Kuzmicheva, E. N. Domoroschina, V. B. Rybakov, A. B. Dubovsky, E. A. Tyunina, *J. Crystal Growth* **275**, e715 (2005).
- [10] T. Bodziony, S. M. Kaczmarek, W. Ryba-Romanowski, M. Berkowski, *Proc. SPIE* **5958**, 595827 (2005).

\*Corresponding author: ana.voiculescu@inflpr.ro